

# Magnetically- and Electrically-Controllable Functional Liquid Metal Droplets

Fangxia Li, Shaolong Kuang, Xiangpeng Li,\* Jian Shu, Weihua Li, Shi-Yang Tang,\* and Shiwu Zhang\*

Gallium-based room temperature liquid metal alloys have recently been explored to be an emerging functional material. They have attracted particular attentions in a variety of applications due to their unique properties. Many of the applications are based on the precise control over the motion of liquid metal, and yet, the fact that currently lacking the advanced and reliable controlling methods greatly hinders the potential of liquid metal to be applied in a wider range of fields. In this study, an innovative approach is developed to obtain functional liquid metal (FLM) by modifying it with copper–iron magnetic nanoparticles (Cu–Fe NPs). The magnetic modification process enables the Cu–Fe NPs to be suspended within the liquid metal and form the FLM. The FLM exhibits similar appearance, actuating behaviors, and deformability in alkaline solutions to those of pure liquid metal alloys. Meanwhile, the magnetic modification enables the precise and rapid manipulation of the liquid metal using a magnetic field. Most importantly, for the first time, the precise control and climbing locomotion of the FLM is demonstrated with the interworking of both electric and magnetic fields simultaneously. The remarkable features of the FLM may represent vast potentials toward the development of future intelligent soft robots.

including microelectromechanical (MEMS) actuators,<sup>[8–12]</sup> microscale heat exchangers,<sup>[13,14]</sup> soft and wearable electronics,<sup>[15–19]</sup> and reconfigurable structures.<sup>[20,21]</sup> Several techniques have been developed to control the motion and deformation of liquid metal droplets. Applying an external potential gradient is the most commonly used method to drive and deform liquid metal within electrolytes.<sup>[8,9,12,22]</sup> Other approaches for driving liquid metal droplets by inducing chemical reactions,<sup>[23,24]</sup> and ionic imbalance<sup>[25]</sup> have also been demonstrated. Recently, the actuation of liquid metal droplets using external magnetic fields has been explored through the modification of liquid metal surface with ferromagnetic materials. For example, liquid metal coated with iron (Fe) nanoparticles (NPs) can be manipulated, merged, and separated in microfluidic channels with various angles in discretionary direction using an external magnetic field.<sup>[26]</sup>


## 1. Introduction

Gallium-based room temperature liquid metal alloys such as Galinstan or EGaIn are becoming emerging functional materials in recent years, and have drawn considerable attentions from both of academia and industry.<sup>[1,2]</sup> Such liquid metals possess many extraordinary properties including high surface tension, favorable flexibility, high electrical/thermal conductivities, and much less toxic in comparison to mercury.<sup>[3–7]</sup> Particularly, the mobility and deformability of liquid metal in aqueous environment have been verified to be of a great significance to develop diverse applications

Other ferromagnetic materials such as nickel can be electroplated on the surface of liquid metal to form a motor.<sup>[27]</sup> The liquid metal motor can be controlled using both magnetic and electric fields, and also can achieve autonomous locomotion by reacting with aluminum foil. Similarly, porous structure of liquid metal can be obtained by mixing liquid metal and iron NPs in hydrochloric acid.<sup>[28]</sup> Such a porous mix can expand when subjected to heating to control its density. However, the above-mentioned approaches using electroplating or NP coating/mixing significantly affect the intrinsic properties of liquid metal and may sacrifice the surface fluidity, deformability, and flexibility of the material.

F. Li, Prof. S. Kuang, Prof. X. Li  
College of Mechanical and Electrical Engineering  
Soochow University  
Suzhou 215000, China  
E-mail: licool@suda.edu.cn

Prof. X. Li  
State Key Laboratory of Applied Optics  
Changchun Institute of Optics  
Changchun 130033, China

 The ORCID identification number(s) for the author(s) of this article can be found under <https://doi.org/10.1002/admt.201800694>.

J. Shu, Prof. S. Zhang  
CAS Key Laboratory of Mechanical Behavior and Design of Materials  
Department of Precision Machinery and Precision Instrumentation  
University of Science and Technology of China  
Hefei 230026, China  
E-mail: swzhang@ustc.edu.cn

Prof. W. Li, Dr. S.-Y. Tang  
School of Mechanical  
Materials, Mechatronic and Biomedical Engineering  
University of Wollongong  
Wollongong, NSW 2522, Australia  
E-mail: shiyang@uow.edu.au

DOI: 10.1002/admt.201800694

In this study, we developed a novel method for producing FLM that can be manipulated using both magnetic and electric fields, and yet, the FLM still exhibits similar appearance, mobility, and deformability to those of pure liquid metal. Motivated by the process demonstrated for making magnetic liquid metal,<sup>[29]</sup> we first obtained the liquid metal marble by coating copper–iron (Cu–Fe) NPs on a Galinstan droplet and remove the oxide layer using hydrochloric acid (HCl) solution. The FLM contains magnetic NPs was later separated from the solid shell and collected after applying an external potential gradient within a sodium hydroxide (NaOH) solution. We conducted five proof-of-concept experiments to investigate the properties of the developed FLM: (1) we first studied the composition of the FLM produced using different mass fractions of Cu–Fe NPs; (2) we later used the FLM as the core of a liquid metal enabled pump to validate its surface fluidity; (3) we studied the manipulation of the FLM in crooked channels with different angles using a magnetic field to verify its mobility and deformability; (4) furthermore, we explored the precise manipulation of the FLM in cross-linked channels with the interworking of both electric and magnetic fields; (5) finally, we demonstrated a trivial method to achieve the anti-gravity climbing locomotion

of a FLM droplet by integrating both of electric and magnetic fields.

## 2. Results and Discussion

The magnetic modification process for obtaining the FLM is illustrated in **Figure 1a–e**, which can be specified as the following steps:

- (1) First, we added 80  $\mu\text{L}$  Galinstan liquid metal into a clean beaker using a syringe (Figure 1a). The surface of the Galinstan immediately oxidized when exposed in the air, forming an oxide skin and making the surface much less reflective.<sup>[26,29–31]</sup>
- (2) Next, we added 50 mg Cu–Fe NPs (Cu:Fe = 3:2) and shook the beaker until the surface of Galinstan was coated with a uniform layer of Cu–Fe NPs (Figure 1b). Due to the oxide layer on both of the Galinstan and the Cu–Fe NPs, the NPs can only stick to the oxide skin of the liquid metal and cannot break through the oxide layer to be suspended within the bulk liquid metal.<sup>[29]</sup>

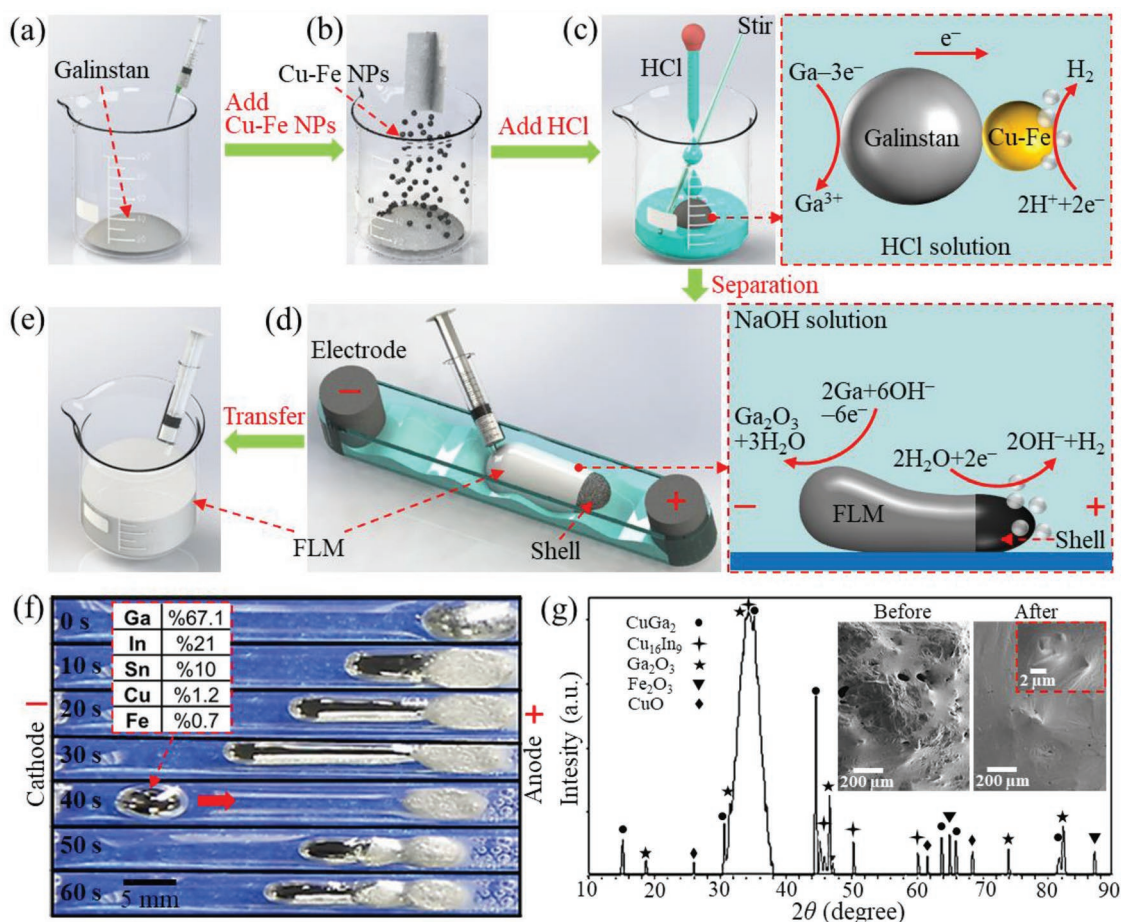


**Figure 1.** Production of the FLM. a–e) Schematic of the modification process for producing the FLM. f) Snapshots of the separation process for obtaining FLM under a 10 V DC voltage in NaOH solution, the inset shows the content of elements detected within the FLM. g) XRD spectrum of the solid shell, the insets show the SEM images of the Galinstan–Cu–Fe NP mix before and after the electrochemistry-assisted separation process.

- (3) After coating the Galinstan with Cu–Fe NPs, diluted HCl solution (8 wt%) was added into the beaker to remove the oxide layer at the surface of Galinstan and the Cu–Fe NPs (Figure 1c); this process facilitates the Cu–Fe NPs to be mixed with Galinstan directly as the NPs surface becomes metallic and more polarizable.<sup>[32–35]</sup> When the Cu–Fe NPs coated Galinstan droplet is immersed into the HCl solution, the Ga and the Cu–Fe NPs coating tend to form a galvanic cell, in which Ga acts as the cathode and Cu–Fe NPs work as anodes, as illustrated in Figure 1c. The galvanic cell oxidizes Ga and protects the Cu–Fe NPs from dissolving by the HCl solution. After vigorously stirring the Galinstan–NPs mix in HCl solution for 30 min until the HCl solution becoming transparent, we found that the surface of Galinstan was covered by a thick layer of solid shell.
- (4) The electrochemistry-assisted sorting process was later adopted to remove the solid shell for obtaining the FLM, as illustrated in Figure 1d,e. The Galinstan–NPs mix was placed in a straight channel and we observed the separation of the solid shell from the inside liquid metal upon the application of a 10 V DC voltage. When the liquid metal stopped flowing, a syringe was used to collect the liquid metal, which is termed as the functional liquid metal, into a container for further experiments. Bipolarization of the liquid metal occurred during the separation process; we observed the generation of gas bubbles on the solid shell (cathodic pole) due to the reduction of water, while the liquid metal on the anodic pole should be oxidized (Figure 1d).

Figure 1f shows the snapshots taken during the separation process (also see Movie S1 in the Supporting Information), from which we can see the elongation of liquid metal towards the cathode from the less-reflective solid shell in the beginning. The elongation of the liquid metal is probably due to the oxidation of the liquid metal at the anodic pole, and such an oxidation process lowers its effective interfacial tension.<sup>[36–38]</sup> Therefore, this may generate a Marangoni flow travelling towards the area with a higher interfacial tension (cathodic pole) to drag the liquid metal toward the cathode.<sup>[39]</sup> As such, liquid metal can be successfully separated from the solid shell. We observed the separation of liquid metal from the solid shell  $\approx 40$  s after applying the voltage (Figure 1f), and the liquid metal droplet immediately actuated toward the anode similar to the behaviors of bare Galinstan droplets.<sup>[12,22]</sup> Interestingly, once the liquid metal droplet hits the solid shell, it merges back to the solid shell and drags it towards the cathode. These elongation, breaking, back-actuation, merging, and dragging processes keep repeating until the solid shell touches the cathode (see Movie S1 in the Supporting Information). We performed energy-dispersive X-ray spectroscopy (EDS) analysis to investigate the components of the separated FLM, and the content of the detected elements are listed in the inset of Figure 1f. We can see that the FLM contains a small amount of Cu and Fe, while the mass ratio among Ga, In, and Sn is very close to that of Galinstan. We later demonstrated that such a small amount of Fe is enough to make the liquid metal ferromagnetic, and meanwhile maintains the liquidity of the material.

We further conducted X-ray diffraction (XRD) analyses to identify the components within the solid shell after separation, as shown in Figure 1g. The spectrum shows that the solid shell contains Cu–Ga and Cu–In alloys, as well as oxides of Ga, Cu, and Fe. We believe the existence of the intermetallic  $\text{CuGa}_2$  is benefit for the suspending of Cu–Fe NPs within Galinstan to form stable functional liquid metal.<sup>[40]</sup> We also obtained SEM images of the Galinstan–NP mix before and after electrochemistry-assisted separation, as shown in the insets of Figure 1g, in which we can clearly see that the surface of the mix is porous and rough before separation, while the FLM after separation exhibits a much smoother surface. However, we are still able to observe the existence of the suspended Cu–Fe NPs (see the zoomed in image). The liquidity of the liquid metal, together with the suspended Cu–Fe NPs, enables the unique properties of the FLM that can be harnessed for manipulation using both electrical and magnetic approaches.

Actually, not all the added Cu–Fe NPs can be suspended within the FLM after the electrochemical separation process. Therefore, we measured the accurate mass fraction of the Cu–Fe NPs in the FLM with respect to the amount of NPs originally added to the 80  $\mu\text{L}$  Galinstan, as given in Figure 2a. We found that the mass fraction of the Cu–Fe NPs in the FLM was saturated at  $\approx 9.97$  wt% and can no longer be increased despite of adding more Cu–Fe NPs. The electrical conductivity increases for FLM with a higher mass fraction of the Cu–Fe NPs. This is probably due to the fact that the suspended Cu–Fe NPs have a higher electrical conductivity than that of Galinstan. Meanwhile, from the electrochemical oxidation experiments using a Galinstan and a FLM droplet,<sup>[38]</sup> we found that the surface tension of the FLM is slightly lower than that of Galinstan at the same oxidative potential (see Figure S1 in the Supporting Information).

To employ the liquidity of the obtained FLM droplet for realizing its electrical control, we conducted a series of experiments to explore the influence of different mass fractions of Cu–Fe NPs on the mobility of the FLM droplets during their electrical actuation in NaOH solution. We conducted experiments using a straight channel (length and width of 80 and 4 mm, respectively) filled with NaOH solution ( $0.5 \text{ m L}^{-1}$ ), and the volume of the FLM droplets was 50  $\mu\text{L}$ . We observed that the FLM droplet always moves towards the anode upon the application of a DC voltage, and the velocity–voltage relationship of the FLM droplets with different mass fractions of Cu–Fe NPs is shown in Figure 2b. It requires less voltage ( $\approx 4$  V) to start actuating bare Galinstan droplet, and a larger voltage is needed to drive the FLM droplet with a higher mass fraction of Cu–Fe NPs (e.g.,  $\approx 8$  V for the case of 9.97 wt% Cu–Fe NPs). The speed of the droplets increases almost linearly with the applied voltage, reaching a saturation point at  $\approx 16$  V, after which we did not observe a significant increase in speed.

The electrical actuation of the FLM droplet is due to the Marangoni effect induced by the generation of a nonuniform surface tension profile at the FLM–solution interface upon the application of an external potential gradient.<sup>[9,12]</sup> Assuming that the FLM droplet is spherical and neglecting the frictional force between the droplet and the substrate, the actuating speed of the FLM droplet can be expressed as<sup>[41]</sup>



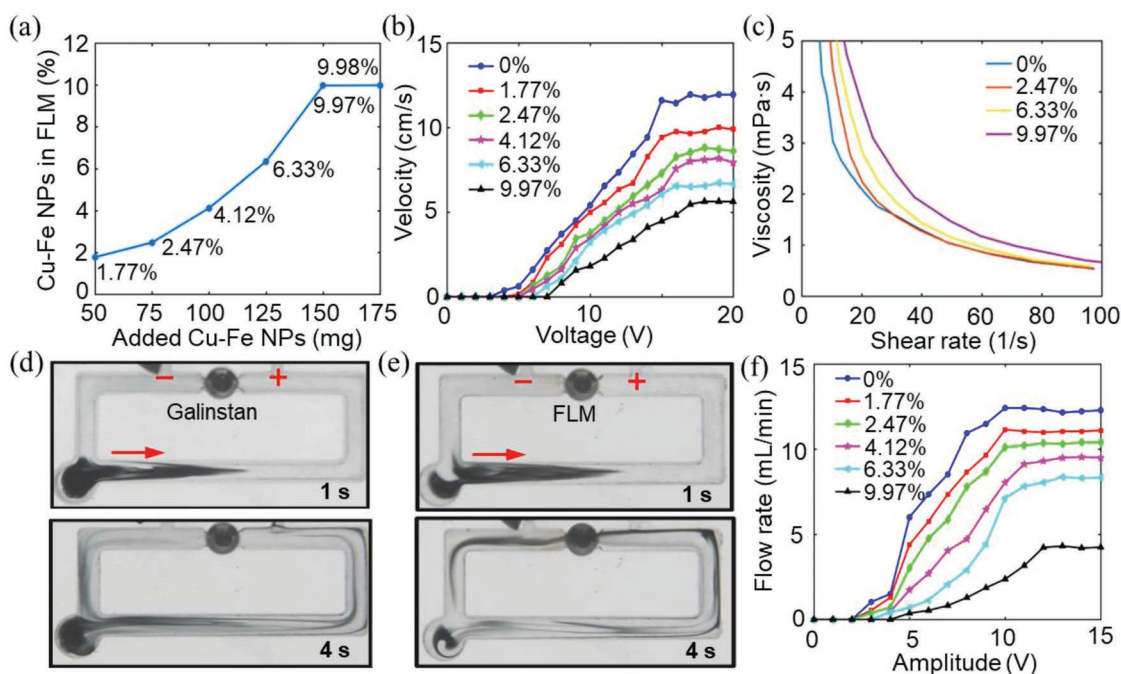


**Figure 2.** Electrical control of the FLM. a) Plot of the actual mass fraction of the Cu–Fe NPs within the FLM after the separation process versus mass of the initially added Cu–Fe NPs. b) Plot of locomotion velocity versus applied DC voltages for the FLM droplets. c) Viscosity versus shear rate for Galinstan and FLM containing 2.47, 6.33, and 9.97 wt% of Cu–Fe NPs. d,e) Sequential snapshots for the pumping effect of a Galinstan and FLM (2.47% Cu–Fe NPs) droplet, respectively, with the application of a square wave signal (200 Hz, 5 V<sub>p-p</sub>, 2.5 V DC offset and 50% duty cycle). f) Plot of pumping flow rate versus signal amplitude for Galinstan and FLM droplets.

$$V = \left| \frac{-1}{4\pi R(2\eta_{\text{NaOH}} + 3\eta_{\text{FLM}})} \iint \nabla_s \sigma \, dA \right| \quad (1)$$

where  $V$  and  $R$  are the actuating speed and the radius of the FLM droplet, respectively;  $\eta_{\text{NaOH}}$  and  $\eta_{\text{FLM}}$  denote the viscosity of the surrounding NaOH solution and the FLM, respectively;  $\sigma$  is the interfacial tension between the FLM and the NaOH solution,  $dA$  is the infinitesimal surface area of the droplet and  $\nabla_s \sigma$  represents the surface-tension gradient over the whole droplet surface. From Equation (1) we can see that upon the application of a larger voltage, a higher actuating speed can be induced for the FLM droplet by generating a larger surface-tension gradient  $\nabla_s \sigma$ .<sup>[9]</sup> In addition, from Figure 2b we can clearly see that the actuating speed reduces when increasing the mass fraction of the Cu–Fe NPs in the FLM droplets. According to Equation (1), we believe the decrease in speed is due to the increased viscosity of the FLM ( $\eta_{\text{FLM}}$ ) with a higher mass fraction of the Cu–Fe NPs. This is evidenced by our viscosity measurements for Galinstan and the FLM with the mass fractions of 2.47, 6.33, and 9.97 wt%, as shown in Figure 2c.

Previous studies report that liquid metal may lose its liquidity after mixing with ferromagnetic materials due to the formation of alloy.<sup>[27,28]</sup> Our experimental results show no increase in viscosity for the FLM after exposing it to air for more than 120 h (See Figure S2 in the Supporting Information). This is due to the fact that the self-limiting gallium oxide layer formed on the surface of the FLM can protect the liquid FLM inside from further oxidation.<sup>[3]</sup> To further demonstrate the fluidity of the FLM, we utilized a droplet of the FLM as the core of the liquid metal

enabled pump for pumping NaOH solution (0.5 M) within a closed-loop channel and compared its pumping performance with bare Galinstan.<sup>[9]</sup> Figure 2d,e shows the snapshots of the pumping effect for a Galinstan and FLM droplet (2.47 wt% Cu–Fe NPs), respectively (see Movie S2 in the Supporting Information). We used a droplet of black dye to indicate the pumping effect, and we can see that Galinstan droplet can induce a slightly higher flow rate (12 mL min<sup>−1</sup>) than that of the FLM droplet (11 mL min<sup>−1</sup>). Figure 2f characterizes the continuous pumping effect of the FLM droplets with different Cu–Fe-NP contents in response to the external voltage of different amplitudes (200 Hz, square wave with an amplitude/2 DC offset). We found that the pumping performance is compromised for FLM droplets with higher Cu–Fe NP contents due to their larger viscosities. These results clearly prove that the FLM can retain the surface fluidity of liquid metal.

We discovered that the FLM can also be controlled using magnetic field despite its low content of Cu–Fe NPs. We firstly conducted a series of experiments to study the intensity of the magnetic field required for driving the FLM droplets with various mass fractions of Cu–Fe NPs, and the experimental setup is shown in Figure 3a. A FLM droplet (volume of 100  $\mu$ L) was placed on the bottom of a Petri dish filled with NaOH solution (0.5 M). We placed a magnet under the Petri dish and made it slowly approach the FLM droplet, while the probe of a gauss meter was fixed under the FLM droplet to record the minimum magnetic flux density  $B$  required to drive the FLM droplet. Figure 3b shows the measured minimum  $B$  with respect to the FLM droplets of different contents of Cu–Fe NPs. The droplets can be actuated using a small  $B$  (<100 Gs) due to the presence

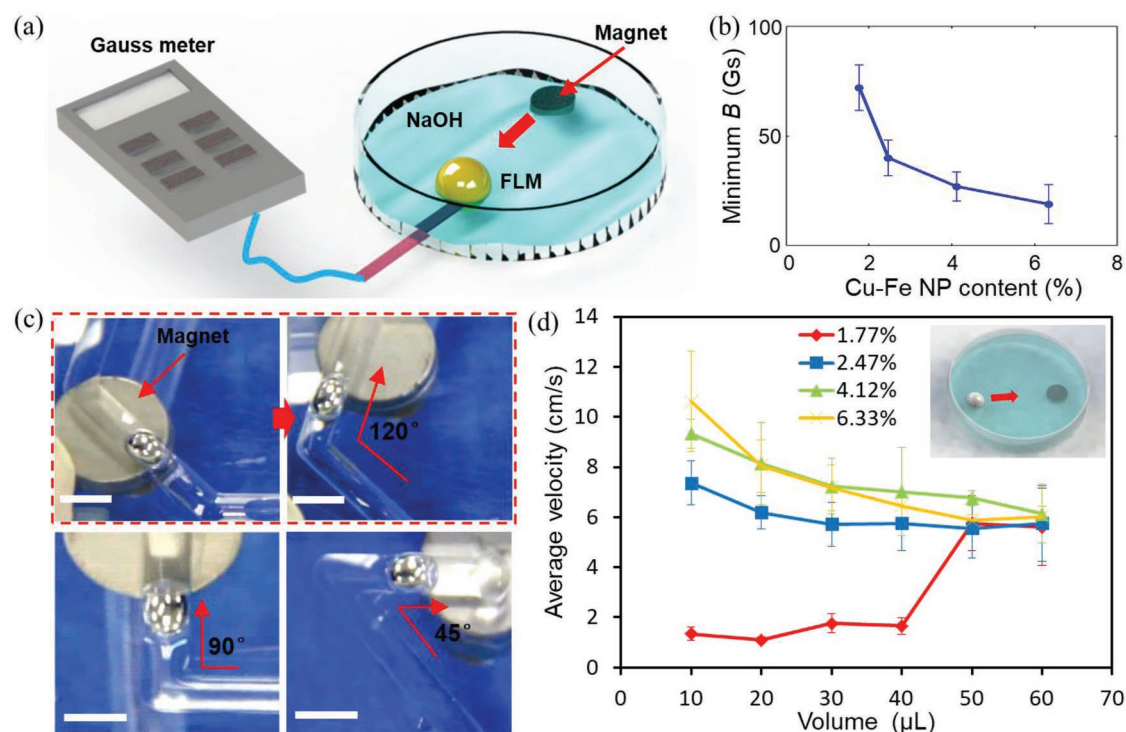


**Figure 3.** Control of the FLM using magnetic field. a) Schematic of the experimental setup for investigating the minimum intensity of  $B$  required for driving the FLM droplets. b) Plot of the minimum  $B$  required for driving a FLM droplet (volume of 100  $\mu\text{L}$ ) versus contents of Cu–Fe NPs within the droplet. c) Manipulating the FLM droplet in crooked channels using a magnet. d) Average actuating velocity versus droplet volume for FLM droplets with different Cu–Fe NP contents. Scale bars are 5 mm.

of a slip layer between the FLM and the substrate, and the minimum  $B$  required to drive the FLM droplet reduces with the increased mass fraction of Cu–Fe NPs. As such, we further demonstrated the controlled actuation of a FLM droplet (2.47 wt% Cu–Fe NPs) within crooked channels using magnetic field, as shown in Figure 3c (also see Movie S3 in the Supporting Information), in which we can see that the FLM droplet can successfully pass through the turns with different angles. These experiments reveal that the FLM droplet exhibits a good deformability and can be manipulated within a limited space using magnetic field.

Next, we conducted a series of experiments to study the actuating velocity of the FLM droplets under an external magnetic field. In doing so, we used FLM droplets (volumes ranging from 10 to 60  $\mu\text{L}$ ) with different contents of Cu–Fe NPs for the experiment. We fixed a magnet ( $B \approx 3500$  Gs) under the Petri dish filled with NaOH solution (0.5 M), and a FLM droplet was placed 30 mm away from the magnet (the inset of Figure 3d shows the experimental setup). The FLM droplet experienced a magnetic force and moved towards the magnet. Figure 3d shows the calculated average velocity of the FLM droplets with respect to their sizes. In general, higher actuating speeds can be induced for FLM droplets with higher Cu–Fe NP contents. For FLM droplets with a low Cu–Fe NP content of 1.77 wt%, the increase in velocity for droplets with larger sizes is probably because larger droplets have more Cu–Fe NPs and therefore, can experience a larger magnetic force. However, for FLM droplets with higher NP contents, a decrease in velocity when increasing the size was observed (Figure 3d). Since higher Cu–Fe NP content

can lower the surface fluidity of the FLM (see Figure 2b,c,f); consequently, this could induce a larger friction between the droplets and the Petri dish. Therefore, as we increase the size of the FLM droplet, the frictional force may increase faster than the magnetic driving force to lower the velocity.

After investigating the control of the FLM using magnetic field, we designed a proof-of-concept experiment to explore the manipulation of the FLM using both electric and magnetic fields simultaneously. In doing so, we added FLM droplet (volume of 50  $\mu\text{L}$ , 2.47 wt% of Cu–Fe NPs) into a cross-linked channel filled with NaOH solution (0.5 M), as shown in Figure 4a. The channel has eight graphite electrodes; we assigned Electrode 1 as the cathode and the rest of the electrodes as the anode. From our experiment we observed that the FLM droplet initially actuated from Electrode 1 towards the anode of the cross-linked channel upon the application of a 10 V voltage. Interestingly, the FLM droplet stopped moving when reaching the intersection of the channel (Figure 4b). This can be attributed to the fact that the FLM droplet reached the equilibrium position where the surface tension induced forces exerted on the droplet at each direction are balanced due to the symmetric arrangement of the electrodes (also see Movie S4 in the Supporting Information). Such a balancing situation could happen when manipulating liquid metal droplets electrically in a complex system where multiple electrodes may be activated at the same time. We hypothesize that the balance can be broken by introducing a magnetic force on the FLM droplet, and we can guide the droplet towards any desired anode (Figure 4a). We examined our hypothesis by placing a permanent magnet under the channel next to the equilibrium position

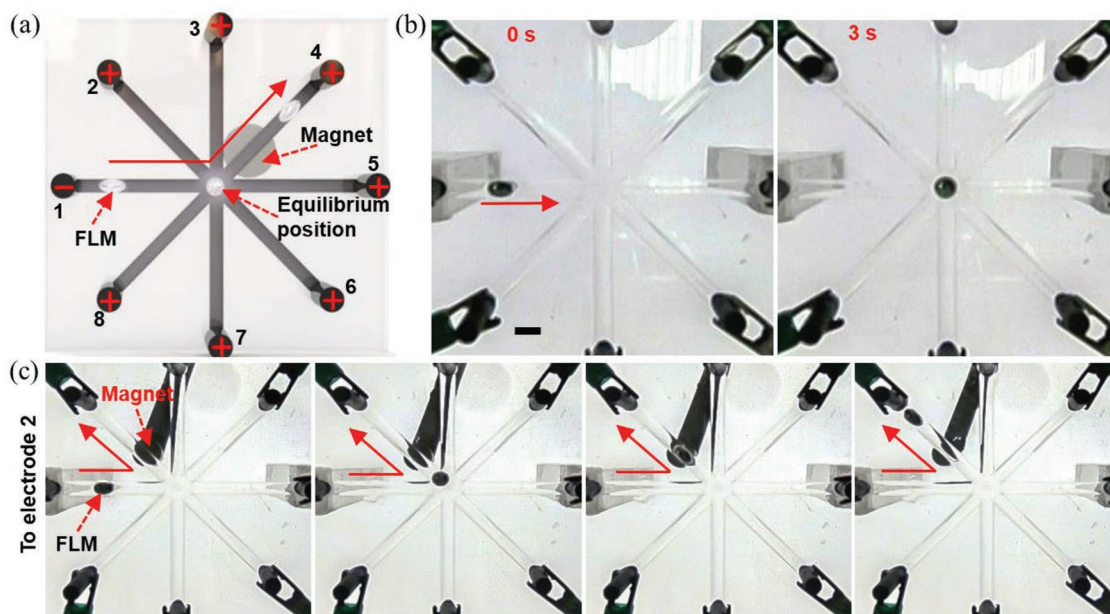


**Figure 4.** Control of the FLM using both electric and magnetic fields. a) Schematic of the experimental setup for demonstrating the control of the FLM droplet in a cross-linked channel using both electric and magnetic fields. b) Sequential snapshots for the case when the FLM droplet stops moving after reaching the equilibrium position. c) Snapshots showing the example of controlling the actuating direction for a FLM droplet using both electric and magnetic fields. Scale bars are 5 mm.

before applying the voltage. The additional magnetic force exerted on the droplet can break the balance at the equilibrium position and guide the droplet towards the desired direction, as shown in Movie S4 in the Supporting Information. Figure 4c shows the example of actuating a FLM droplet towards Electrode 2 upon the application of both electric and magnetic fields. The FLM droplet initially moved from Electrode 1 towards the equilibrium position at an average speed of  $\approx 9 \text{ cm s}^{-1}$ , and then the droplet was directed towards Electrode 2 at an average speed of  $\approx 6 \text{ cm s}^{-1}$ . The magnetic field induced force exerted on the FLM droplet at the equilibrium position was estimated by calculating the acceleration ( $\approx 450 \text{ cm s}^{-2}$ ) of the droplet (mass of  $\approx 314 \text{ mg}$ ) from Movie S4 (Supporting Information), and the estimated force is  $\approx 1.4 \text{ N}$ .

Due to the high density of liquid metal, most of the liquid metal droplets or devices can only move in plane. Out-of-plane actuation of liquid metal using continuous electrowetting effect (CEW) within a sub-millimeter sized channel was recently demonstrated.<sup>[42]</sup> However, the climbing locomotion of free-standing liquid metal droplets without the confinement of channel is still underexplored. Based on our experimental results, we found that it is very difficult for a liquid metal droplet to climb a slope when only actuated electrically. Figure 5a shows that the Galinstan droplet (volume of  $50 \text{ }\mu\text{L}$ ) failed to climb the slope with a small angle of inclination ( $10^\circ$ ) upon the application of a  $15 \text{ V}$  DC voltage to the electrodes ( $90 \text{ mm}$  apart). Similarly, the FLM droplet (volume of  $50 \text{ }\mu\text{L}$ ,  $2.47 \text{ wt\%}$  of Cu–Fe NPs) also stopped at the foot of the slope, as shown in Figure 5b. This proves that the driving force induced by an external potential gradient is unable to overcome gravity and accomplish the climbing locomotion. However, the advantage of this FLM is that an additional magnetic force can be exerted on the droplet along the vertical direction. The climbing locomotion of the FLM droplet can be successfully accomplished by activating the

electromagnet ( $B \approx 450 \text{ Gs}$ ) above the slope while applying a  $15 \text{ V}$  DC voltage to the electrodes, as shown in Figure 5c (also see Movie S5 in the Supporting Information). The FLM droplet initially actuated towards the foot of the slope at an average speed of  $\approx 10 \text{ cm s}^{-1}$  upon the application of the DC voltage, and then the FLM droplet started to climb the slope at an average speed of  $\approx 11 \text{ cm s}^{-1}$  with the assistance of the magnetic field. When the FLM droplet reached the top of the slope, the electromagnet was deactivated and the FLM droplet continued to move towards the anode at an average speed of  $\approx 8 \text{ cm s}^{-1}$ .

### 3. Conclusion

In summary, we developed a novel method for producing FLM comprising Galinstan and Cu–Fe NPs that can be manipulated using both magnetic and electric fields. We demonstrated the production process and explored the properties of the FLM. We found that using the innovative electrochemistry-assisted separation process, the produced FLM has similar appearance, mobility, and deformability to those of pure liquid metal. We further investigated the electrical and magnetic actuation of the FLM droplets with different contents of Cu–Fe NPs. Most importantly, we discovered that the locomotion of this FLM can be controlled by the interworking of both electric and magnetic fields simultaneously. This enables the precise manipulation of the actuating direction within a cross-linked channel, as well as the climbing locomotion of the FLM droplets. The feasibility of the production process, together with the highly controllable actuating behaviors presented for this FLM, could enable the potential for developing liquid metal based soft robots for various applications, such as soft tools for surgery and drug delivery with untethered and remotely controllable manners.<sup>[43]</sup>



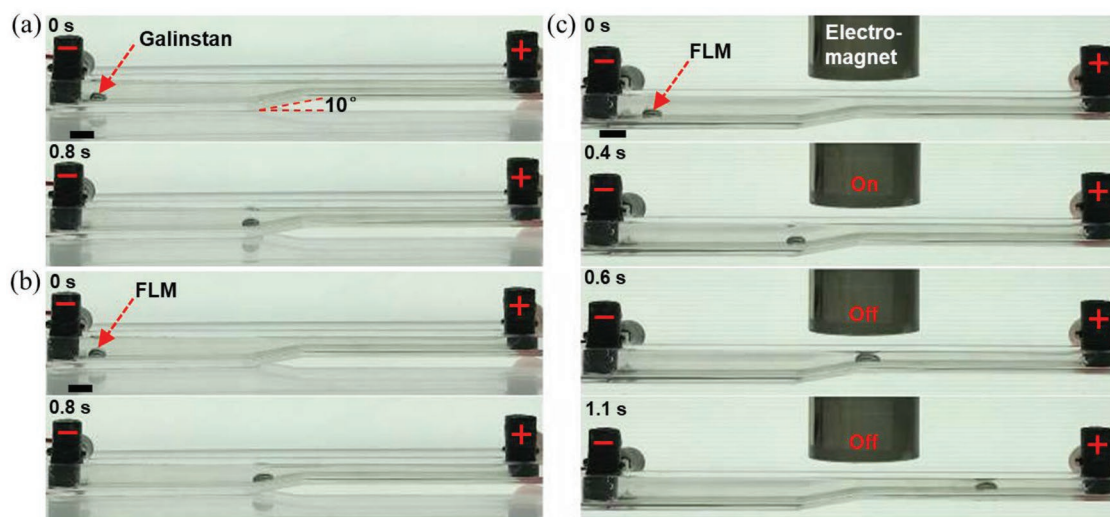


**Figure 5.** Climbing locomotion of the FLM droplet. Unsuccessful climbing locomotion of a) a Galinstan droplet, and b) a FLM droplet upon the application of a 15 V electrical potential between the electrodes. c) Successful climbing locomotion of the FLM droplet with the assistance of a magnetic force.

## 4. Experimental Section

**Materials:** Galinstan alloy (67% Ga, 20.5% In, and 12.5% Sn), was used as the metallic liquid base. Copper–iron (Cu–Fe) NPs (diameter of 100 nm, Shanghai Yu-sui Welding Material) with different mass fraction of copper were chosen as the packing material. The electrolyte used in all experiments was NaOH aqueous solution (0.5 M).

**Fabrication of Channels:** Four types of channels were adopted in experiments for evaluating the properties of the FLM, including straight channels, a crooked channel with different angles, a cross-linked channel with eight-linked branch channels, and a straight channel with a slope (10° angle of inclination). All these channels were fabricated by milling transparent polymethylmethacrylate (PMMA).

**Generating Magnetic Field and Electric Field:** The magnetic fields in the experiments were generated by a commercially available neodymium–iron–boron (NdFeB) permanent magnet (maximum magnetic flux density of 3500 Gs) and an electromagnet (P34/25, Fanke Electric Company, China). The DC voltages were provided by a DC power supply (IT6432, ITECH, China). The alternating voltages were imposed by alternating power supply (APS-1102A, GW INSTEK, China). All the electrodes were graphite electrodes.

**Videos and Photos:** Videos were captured by a camera (Canon EOS-550D, Japan). The transient images, velocity data, and the appearance of the FLM were extracted from videos. Scanning electron microscopy (SEM) images were taken using a Merlin Compact SEM (Zeiss, Germany). The X-ray diffraction (XRD) data was obtained using an X-ray diffraction system (Ultima IV, Rigaku, Japan) at ambient temperature. The viscosity of liquid metal was measured using a rheometer (AR2000, TA instruments, America).

**Electrical Conductivity Characterization:** A Source Measure Unit (2614B, Keithley, America) was adopted to quantitatively measure the electrical resistivity of Galinstan and the FLM. In doing so, a droplet of Galinstan or the FLM was used to fill a PMMA cylindrical container (radius and height are both 5 mm), and a pair of electrodes were attached to the top and bottom of the container to obtain the resistivity.

## Supporting Information

Supporting Information is available from the Wiley Online Library or from the author.

## Acknowledgements

F.L. and S.K. contributed equally to this work. This work was supported in part by grants from NSFC under Grant Nos. 61503270, 51828503, 61873339, a grant from National Science Foundation of Jiangsu Province under Grant No. BK20150326, a grant from National Science Foundation for Colleges and Universities of Jiangsu Province under Grant No. 15KJB510029, a grant from China Postdoctoral Science Foundation under Grant No. 2016M590497, and supported by the State Key Laboratory of Applied Optics. Dr. Shi-Yang Tang is the recipient of the Vice-Chancellor's Postdoctoral Research Fellowship funded by the University of Wollongong.

## Conflict of Interest

The authors declare no conflict of interest.

## Keywords

field-responsive material, functional materials, galinstan, liquid metals, locomotion

Received: December 7, 2018

Revised: January 8, 2019

Published online: January 22, 2019

- [1] M. D. Dickey, *Adv. Mater.* **2017**, 29, 1606425.
- [2] T. Liu, P. Sen, C. J. Kim, *J. Microelectromech. Syst.* **2012**, 21, 443.
- [3] M. D. Dickey, *ACS Appl. Mater. Interfaces* **2014**, 6, 18369.
- [4] S.-Y. Tang, B. Ayan, N. Nama, Y. Bian, J. P. Lata, X. Guo, T. J. Huang, *Small* **2016**, 12, 3861.
- [5] N. Kazem, T. Hellebrekers, C. Majidi, *Adv. Mater.* **2017**, 29, 1605985.
- [6] T. Daeneke, K. Khoshmanesh, N. Mahmood, I. A. De Castro, D. Esrafilzadeh, S. J. Barrow, M. D. Dickey, K. Kalantar-Zadeh, *Chem. Soc. Rev.* **2018**, 47, 4073.
- [7] J. Yan, Y. Lu, G. Chen, M. Yang, Z. Gu, *Chem. Soc. Rev.* **2018**, 47, 2518.

- [8] J. Wu, S.-Y. Tang, T. Fang, W. H. Li, X. P. Li, S. W. Zhang, *Adv. Mater.* **2018**, *30*, 1805039.
- [9] S.-Y. Tang, K. Khoshmanesh, V. Sivan, P. Petersen, A. P. O'Mullane, D. Abbott, A. Mitchell, K. Kalantar-zadeh, *Proc. Natl. Acad. Sci. USA* **2014**, *111*, 3304.
- [10] M. D. Bartlett, N. Kazem, M. J. Powellpalm; X. Huang, W. Sun, J. A. Malen, C. Majidi, *Proc. Natl. Acad. Sci. USA* **2017**, *114*, 2143.
- [11] J. Shu, S.-Y. Tang, Z. H. Feng, W. H. Li, X. P. Li, S. W. Zhang, *Soft Matter* **2018**, *14*, 7113.
- [12] S.-Y. Tang, V. Sivan, K. Khoshmanesh, A. P. O'Mullane, X. Tang, B. Gol, F. Eshtiaghi, N. Lieder, P. Perersen, A. Mitchell, K. Kalantar-zadeh, *Nanoscale* **2013**, *5*, 5949.
- [13] M. Garc a, J. Orozco, M. Guix, W. Gao, S. Sattayasamitsathit, A. Escarpa, *Nanoscale* **2013**, *5*, 1325.
- [14] J. Darabi, M. M. Ohadi, D. Devoe, *J. Microelectromech. Syst.* **2001**, *10*, 98.
- [15] Y. Lin, C. Cooper, M. Wang, J. J. Adams, J. Genzer, M. D. Dickey, *Small* **2015**, *11*, 6397.
- [16] T. Lu, E. Markvicka, Y. Jin, C. Majidi, *ACS Appl. Mater. Interfaces* **2017**, *9*, 22055.
- [17] N. Ilyas, A. Cook, C. E. Tabor, *Adv. Mater. Interfaces* **2017**, *4*, 1700141.
- [18] K. B. Ozutemiz, J. Wissman, O. B. Ozdoganlar, C. Majidi, *Adv. Mater. Interfaces* **2018**, *5*, 1701596.
- [19] R. Matsuzaki, K. Tabayashi, *Adv. Funct. Mater.* **2015**, *25*, 3797.
- [20] E. Palleau, S. Reece, S. C. Desai, M. E. Smith, M. D. Dickey, *Adv. Mater.* **2013**, *25*, 1589.
- [21] M. Kelley, C. Koo, H. Mcquilken, B. Lawrence, *Electron. Lett.* **2013**, *49*, 1370.
- [22] B. L. Cumby, G. J. Hayes, M. D. Dickey, R. S. Justice, C. E. Tabor, J. C. Heikenfeld, *Appl. Phys. Lett.* **2012**, *101*, 277.
- [23] X. Tang, S.-Y. Tang, V. Sivan, K. Khoshmanesh, *Appl. Phys. Lett.* **2013**, *103*, 8432.
- [24] J. Zhang, Y. Yao, L. Sheng, J. Liu, *Adv. Mater.* **2015**, *27*, 2648.
- [25] A. Zavabeti, T. Daeneke, A. F. Chrimes, A. P. O'Mullane, O. J. Zhen, A. Mitchell, K. Khoshmanesh, K. Kalantar-zadeh, *Nat. Commun.* **2016**, *7*, 12402.
- [26] J. Jeon, J. B. Lee, S. K. Chung, D. Kim, *Lab Chip* **2017**, *17*, 128.
- [27] J. Zhang, R. Guo, J. Liu, *J. Mater. Chem. B* **2016**, *4*, 5349.
- [28] H. Wang, B. Yuan, S. Liang, R. Guo, W. Rao, X. L. Wang, H. Chang, Y. J. Ding, J. Liu, L. Wang, *Mater. Horiz.* **2018**, *5*, 222.
- [29] F. Carle, K. Bai, J. Casara, K. Vanderlick, E. Brown, *Phys. Rev. Fluids* **2017**, *2*, 013301.
- [30] M. J. Regan, H. Tostmann, P. S. Pershan, O. M. Magnussen, E. Dimasi, B. M. Ocko, *Phys. Rev. B* **1997**, *55*, 10786.
- [31] Q. Xu, N. Oudalov, Q. Guo, H. M. Jaeger, E. Brown, *Phys. Fluids* **2012**, *24*, 299.
- [32] D. Kim, P. Thissen, G. Viner, D. W. Lee, W. Choi, Y. J. Chabal, *ACS Appl. Mater. Interfaces* **2013**, *5*, 179.
- [33] J. C. Hemmelmann, H. Xu, W. Krumm, *Metall. Mater. Trans. B* **2013**, *44*, 1232.
- [34] H. W. Fox, W. A. Zisman, *J. Colloid Sci.* **1952**, *7*, 428.
- [35] P. G. D. Gennes, F. Brochard-Wyart, D. Qu  r  , *Capillary and Wetting Phenomenon*, Springer, New York **2004**.
- [36] J. Wissman, M. D. Dickey, C. Majidi, *Adv. Sci.* **2017**, *4*, 1700169.
- [37] C. B. Eaker, D. C. Hight, J. D. O'Regan, M. D. Dickey, K. E. Daniels, *Phys. Rev. Lett.* **2017**, *119*, 174502.
- [38] M. R. Khan, C. B. Eaker, E. F. Bowden, M. D. Dickey, *Proc. Natl. Acad. Sci. USA* **2014**, *111*, 14047.
- [39] Y. Y. Yao, J. Liu, *RSC Adv.* **2017**, *7*, 11049.
- [40] Y. Cui, F. Liang, Z. Yang, S. Xu, X. Zhao, Y. Ding, *ACS Appl. Mater. Interfaces* **2018**, *10*, 9203.
- [41] M. Schmitt, H. Stark, *Phys. Fluids* **2016**, *28*, 012106.
- [42] K. J. Sarabia, S. S. Yamada, R. C. Gough, M. R. Moorefield, A. W. Combs, W. A. Shiroma, A. T. Ohta, *Electron. Lett.* **2017**, *53*, 1635.
- [43] M. Cianchetti, C. Laschi, A. Menciassi, P. Dario, *Nat. Rev. Mater.* **2018**, *3*, 143.